# Statistical reconstruction of qutrits

Yu. I. Bogdanov
*Russian Control System Agency, "Angstrem," Moscow 124460, Russia*

M. V. Chekhova, L. A. Krivitsky, S. P. Kulik, A. N. Penin, and A. A. Zhukov*
*Department of Physics, Moscow M.V. Lomonosov State University, 119992 Moscow, Russia*

L. C. Kwek†
*National Institute of Education Nanyang Technological University, 637616 Singapore*

C. H. Oh and M. K. Tey‡
*Department of Physics, Faculty of Science, National University of Singapore, 117542 Singapore*
(Received 16 April 2004; published 5 October 2004)

We discuss a procedure of measurement followed by the reproduction of the quantum state of a three-level optical system—a frequency—and spatially degenerate two-photon field. The method of statistical estimation of the quantum state based on solving the likelihood equation and analyzing the statistical properties of the obtained estimates is developed. Using the root approach of estimating quantum states, the initial two-photon state vector is reproduced from the measured fourth moments in the field. The developed approach applied to quantum-state reconstruction is based on the amplitudes of mutually complementary processes. The classical algorithm of statistical estimation based on the Fisher information matrix is generalized to the case of quantum systems obeying Bohr's complementarity principle. It has been experimentally proved that biphoton-qutrit states can be reconstructed with the fidelity of 0.995–0.999 and higher.

DOI: 10.1103/PhysRevA.70.042303 PACS number(s): 03.67.−a, 42.50.Dv

## I. INTRODUCTION

The ability of measuring quantum states is of fundamental interest because it provides a powerful tool for the analysis of basic concepts of quantum theory, such as the fundamentally statistical nature of its predictions, the superposition principle, Bohr's complementarity principle, etc. To measure the quantum state one needs to perform some projective measurements on the state and then to apply some computation procedure to the data. The first step is a genuine measurement consisting of a set of operations on the representatives of a quantum statistical (pure or mixed) ensemble. As a result of such an operation an experimentalist acquires a set of frequencies at which particular events occur. In the second step a mathematical procedure is applied to the statistical data obtained in the previous step to reconstruct the quantum state. Obviously, the complexity of the whole reconstruction procedure depends directly on the minimal number of measurements required for the reconstruction, which, in its turn, is given by the dimensionality of the state Hilbert space.

The necessity of an adequate measurement of the states of such systems is caused not only by fundamental interest but also by some applications. For example, it has been shown that the security of the key distribution in quantum cryptography is associated with the dimensionality of the Hilbert space for the states in use [1]. From this point of view certain hopes are pinned on the three-level systems or qutrits [2–4] rather than qubits.

The present paper is devoted to state reconstruction for the optical three-level systems. The object under study is the polarization state of a frequency and spatially degenerate biphoton field [5,6].

We should mention that there are other implementations of three-level optical systems. The most familiar ones deal with three-arm interferometers [7] and lower-order transverse spatial modes of optical field, realized with holograms [8–10]. Polarization-entangled four-photon fields, which are equivalent to two entangled spin-1 particles, were studied in [11].

All these implementations belong to the art of the modern experimental technique and demonstrate the development of those quantum information branches relating to the practice. However, note that successful manipulation with quantum states implies the ability to control three important stages: state preparation, its transformation, and measurement. From this point of view, biphoton qutrits look quite promising since the mentioned stages are under the full control. The unitary transformations of biphoton polarization states as well as quantum ternary logic have been considered in [12]. Preparation of arbitrary qutrits was realized recently [13], so in the present paper we focus on the complete reconstruction of the biphoton qutrits. Although realistic tomographic procedures for measuring such quantum states were suggested earlier [14–16], this work includes the most advanced approach. Such an approach consists of statistical estimation of the experimental data based on solving the likelihood equation, the so-called root estimation technique [17]. The advantages of the root estimation method are based on the ability

*Electronic address: postmast@qopt.phys.msu.su
†Electronic address: lckwek@nie.edu.sg
‡Electronic address: phyohch@nus.edu.sg, phyteymk@nus.edu.sg

 

to reconstruct the states in the Hilbert space of high dimensionality. The method is asymptotically effective, so it allows one to reconstruct the states with an accuracy that is most close to the accuracy achievable in principle. That is why the formalism applied to the unknown quantum states allowed us to formulate and experimentally check the fundamental statistical limits of the accuracy of state reconstruction. Practically, this is the first application of the root estimation to a large set of experimental data obtained in different regimes of biphoton-state generation, which are widely used in quantum optics and quantum information—namely, speaking about temporal regimes, the data under analysis related to continuous and short-pulsed biphoton sources. As to the polarization regimes, we investigated both types of phase matching (type I and type II) for producing biphotons. Among the works that closely relate to the subject of the present paper and are devoted to state reconstruction, we would like to refer to the family of papers in [18–21], where quantum tomography of qubit pairs was developed. In these works, a detailed analysis of the biphoton polarization states involved in a wide range of processes like decohering, unitary, etc., was implemented. The approach developed in these works exploits the noncollinear (and degenerate) regime for the correlated photon source. Transition to the collinear (and degenerate) regime when biphotons propagate in the single beam rather than in two beams becomes crucial. We put great emphasis on that fact because it makes possible to pass from qubits to qutrits or to a new class of states with higher dimensionality (see Sec. II).

The paper is organized as follows. In Sec. II we discuss the main properties of qutrits based on the polarization state of the biphoton field. We focus on their preparation, visual representation on a Poincaré sphere, and unitary transformation by phase plates. Then we consider the coherence matrix, which characterizes completely the properties of biphoton qutrits in the fourth field moments. Section III is devoted to the methods of biphoton-qutrit measurement; in particular, we introduce two quantum tomography protocols and discuss in detail their experimental implementation. We conclude this part with an analysis of statistical reconstruction for qutrits from the outcomes of mutually complementary measurements. Section IV deals with the methods of quantum-state reconstruction. Namely, we consider the least-squares and maximum-likelihood methods and apply these tools to analysis of the data obtained in quantum tomography. In the Appendix we explore the problem of statistical fluctuations of the state vector which is important for estimation and control of the precision and stability of quantum information.

## II. QUTRITS BASED ON BIPHOTONS

### A. Preparation

Biphoton field is a coherent mixture of two-photon Fock states and the vacuum state [22]:

$$\Psi = |\mathrm{vac}\rangle + \frac{1}{2}\sum_{\vec{k}_s,\vec{k}_i} F_{\vec{k}_s,\vec{k}_i}|1_{\vec{k}_s},1_{\vec{k}_i}\rangle, \tag{1}$$

where $|1_{\vec{k}_s},1_{\vec{k}_i}\rangle$ denotes the state with one (signal) photon in the mode $\vec{k}_s$ and one (idler) photon in the mode $\vec{k}_i$. The coefficient $F_{\vec{k}_s,\vec{k}_i}$ is called the biphoton amplitude [23], because its squared modulus gives a probability to register two photons in modes $\vec{k}_s$ and $\vec{k}_i$.

Let us consider the collinear and frequency-degenerate regime, for which $\vec{k}_s \approx \vec{k}_i$, $\omega_s \approx \omega_i$ and $\omega_s+\omega_i=\omega_p$, where $\omega_p$ is the laser pump frequency. We further restrict our discussion to biphotons that are indistinguishable in terms of spatial, spectral, or temporal parameters. From the point of view of polarization there are three natural states of biphotons: namely, $\Psi_1=|2,0\rangle$, $\Psi_2=|1,1\rangle$, and $\Psi_3=|0,2\rangle$. Here the notation $|2,0\rangle \equiv |2_H,0_V\rangle$, for example, indicates that there are two photons in the horizontal ($H$) polarization mode, while no photons are present in the orthogonal vertical ($V$) mode. These basic states can be generated using type-I (for $\Psi_1$ and $\Psi_3$) and type-II (for $\Psi_2$) phase matching. Since only two-photon Fock states are considered, for the state $|m,n\rangle$ the condition $m+n=2$ must be satisfied.

Any arbitrary pure polarization state of biphoton field can be expressed in terms of three complex amplitudes $c_1, c_2$, and $c_3$:

$$|c\rangle = c_1|2,0\rangle + c_2|1,1\rangle + c_3|0,2\rangle, \tag{2}$$

where $c_j=|c_j|\exp\{i\varphi_j\}$ and $\Sigma_{j=1}^{3}|c_j|^2=1$. The vector $|c\rangle = (c_1,c_2,c_3)$ represents a three-state state or qutrit.

There is an important note concerning the state vector (2). In principle, one can write the complete polarization state in the form

$$|c\rangle = c_1|2_H,0_V\rangle + c_2|1_V,1_H\rangle + c_2'|1_H,1_V\rangle + c_3|0_H,2_V\rangle, \tag{3}$$

where the terms $|1_H,1_V\rangle$ and $|1_V,1_H\rangle$ might be distinguishable somehow, for example, if the photon with vertical polarization comes first with respect to the photon with horizontal polarization. However, we consider a particular two-mode polarization state, so photons differ in polarization only and there are no other parameters responsible for their distinguishability.

In general, to generate an arbitrary qutrit state one needs to put three nonlinear crystals separated in space into a common pump and superpose the biphoton fields generated by the three crystals coherently or incoherently (Fig. 1).

### B. Representation of qutrits using the Poincaré sphere

Sometimes it is very convenient to use a visual representation of the state. For example, a single-photon pure polarization state (qubit) may be mapped onto the Poincaré sphere [three-dimensional (3D) Euclidian sphere]. A (pure) qubit state is determined by polar and azimuthal angles $(\vartheta,\phi)$ in spherical coordinates. Any unitary polarization transformation of the qubit is represented by the corresponding rotation of the sphere. Thus, in order to learn the final transformed state one just has to apply the rotation operation using certain rules.

It would be helpful to use the same visual representation of a qutrit using the Poincaré sphere. Although generalization of the Poincaré sphere for qutrits has been discussed earlier [24] we suggest an alternative approach, which allows us to manipulate with qutrits in natural 3D space rather than in

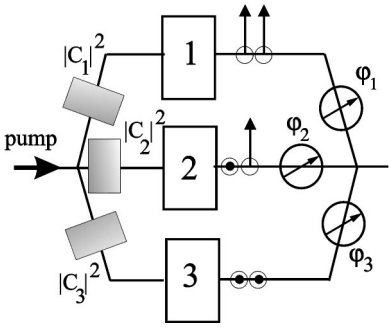


FIG. 1. Preparation of an arbitrary qutrit based on biphotons, in principle. Three nonlinear crystals placed in the common pump generate biphotons with type-I (1, 3) and type-II (2) phase matching. Three attenuators $(|c_1|^2, |c_1|^2, |c_3|^2)$ and three phase shifters $(\varphi_1, \varphi_2, \varphi_3)$ allow one to control three complex amplitudes $c_1$, $c_2$, and $c_3$.

sophisticated 8D space. Let us map the pure polarization state of a biphoton into a pair of points on the sphere (but this is not the two-qubit case since the states $|H,V\rangle$ and $|V,H\rangle$ are indistinguishable). In this representation each photon forming the biphoton is plotted as a single point on the Poincaré sphere, so the qutrit-state vector is represented by

$$|c\rangle = \frac{[a_s^\dagger(\vartheta,\phi)a_i^\dagger(\vartheta',\phi') + a_i^\dagger(\vartheta,\phi)a_s^\dagger(\vartheta',\phi')]|\mathrm{vac}\rangle}{||[a_s^\dagger(\vartheta,\phi)a_i^\dagger(\vartheta',\phi') + a_i^\dagger(\vartheta,\phi)a_s^\dagger(\vartheta',\phi')]|\mathrm{vac}\rangle||}, \tag{4}$$

where $a^\dagger(\vartheta_i,\phi_i)$ and $a^\dagger(\vartheta_s,\phi_s)$ are the creation operators in idler and signal polarization modes and $a^\dagger(\vartheta_m,\phi_m) = \cos(\vartheta_m/2)a^\dagger + e^{i\phi_m}\sin(\vartheta_m/2)b^\dagger$, $m=i,s$. Note that operators $a^\dagger \equiv a_H^\dagger, b^\dagger \equiv a_V^\dagger$ are creation operators for $H$- and $V$-polarized photons.

It is well known that the number of real parameters characterizing a quantum state is determined by the dimension of the Hilbert space $(s)$. For a pure state,

$$N_{pure} = 2s - 2, \tag{5a}$$

and for mixed states,

$$N_{mixed} = s^2 - 1. \tag{5b}$$

According to Eqs. (5a) and (5b), four real parameters determine completely the pure state of a qutrit, so in the Poincaré sphere representation these parameters are simply the four spherical angles $(\vartheta_i,\phi_i;\vartheta_s,\phi_s)$. The links between the angles $(\vartheta_i,\phi_i;\vartheta_s,\phi_s)$ and the amplitudes $c_j = |c_j|\exp i\varphi_j$ are derived in [6]. As an example three basic states $\Psi_1 = |2,0\rangle$, $\Psi_2 = |1,1\rangle$, and $\Psi_3 = |0,2\rangle$ are shown in Fig. 2. It can be shown that the polarization degree of a qutrit $P = \sqrt{|c_1|^2 - |c_3|^2 + 2|c_1^* c_2 + c_2^* c_3|^2}$ [6] has a clear geometrical meaning: it is defined by the angle $\beta$ between the pair of points on the Poincaré sphere as seen from its center:

$$P = \frac{2\cos(\beta/2)}{1+\cos^2(\beta/2)}. \tag{6}$$

For the states $\Psi_1$ and $\Psi_3$ the polarization degree takes values $P_{1,3}=1$, since two points coincide on the sphere and $\beta=0$.

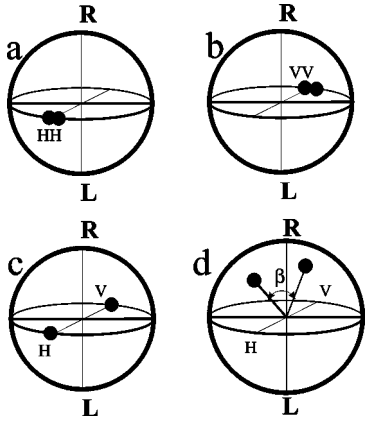


FIG. 2. Representation of a qutrit using the Poincaré sphere. (a), (b), and (c) show three basic states forming superposition (2). (d) represents the state of an arbitrary qutrit.

For the second state, $\Psi_2$, two points are positioned at the opposite sides of the sphere; that is why $\beta/2=\pi/2$ and $P_2 = 0$.

### C. Transformation

Experimentally a unitary transformation of the polarization state (2) can be achieved by placing any retardation plates, rotators, etc., into the biphoton beam. The action of such elements on the state (2) is described by the matrix [12]

$$G = \begin{pmatrix} t^2 & \sqrt{2}tr & r^2 \\ -\sqrt{2}tr^* & |t|^2 - |r|^2 & \sqrt{2}t^* r \\ r^{*2} & -\sqrt{2}t^* r^* & t^{*2} \end{pmatrix}, \tag{7}$$

where

$$t = \cos\,\delta + i\,\sin\,\delta\cos\,2\alpha, \quad r = i\,\sin\,\delta\sin\,2\alpha, \tag{8}$$

$\delta = \pi(n_o - n_e)h/\lambda$ is the optical thickness of the plate, $h$ is its geometrical thickness, and $\alpha$ is the orientation angle between the optical axis of the plate and one of the basis—for example, the vertical direction.

Let us consider the action of the $\lambda/2$ plate on a particular state $\Psi_\perp = (1/\sqrt{2})(|2,0\rangle - |0,2\rangle)$, when the plate is oriented at 22.5°. For the state $\Psi_\perp$ there are two nonzero amplitudes $c_1 = c_3 = 1/\sqrt{2}$ and there is only one relative phase $\varphi_{13} \equiv \varphi_1 - \varphi_3 = \pi$. Taking into account that for a $\lambda/2$ plate $\delta = \pi/2$, the corresponding transmission and reflection coefficients are

$$t = r = \frac{i}{\sqrt{2}}. \tag{9}$$

Thus the matrix $G$ has the form

$$G = \begin{pmatrix} -\frac{1}{2} & -\frac{1}{\sqrt{2}} & -\frac{1}{2} \\ -\frac{1}{\sqrt{2}} & 0 & \frac{1}{\sqrt{2}} \\ -\frac{1}{2} & \frac{1}{\sqrt{2}} & -\frac{1}{2} \end{pmatrix}. \tag{10}$$

Hence, acting by matrix $G$ on the state $\Psi_\perp$ we get

$$G\Psi_\perp = \frac{G}{\sqrt{2}} \begin{pmatrix} 1 \\ 0 \\ -1 \end{pmatrix} = \begin{pmatrix} 0 \\ -1 \\ 0 \end{pmatrix} = \Psi_2.$$

Note that such kind of transformations cannot change the polarization degree of a qutrit. For the state $\Psi_\perp$ chosen above, as well as for the state $\Psi_2$, the polarization degree $P$ is zero.

In the experiment described below we used a simpler way to generate qutrits. Biphotons were produced via collinear frequency-degenerate spontaneous parametric downconversion in a nonlinear crystal (BBO, type-I or type-II phase matching). For type-I phase matching the polarization of both created photons was vertical; i.e., the state $\Psi_3$ was generated. Then, this state was transformed using a quartz plate with a fixed optical thickness. By changing the angle of the plate, the state $\Psi_3 = |0_H, 2_V\rangle$ is transformed according to the formula $|c_{in}\rangle = G\Psi_3$. For the case of type-II phase matching the final state is $|c_{in}\rangle = G\Psi_2$. Of course, the state $|c_{in}\rangle$ does not involve all possible qutrit states because the transformation given by matrix (7) preserves the polarization degree. Anyway, using such a transformation, we select some subset of qutrits to work with.

Such a simple method of state preparation and transformation was chosen in order to be able to compare the results of reconstruction with the parameters of the input states, which should be known with a high accuracy. The purpose of this work is the reconstruction of the initial state $|c_{in}\rangle$.

We would like to emphasize that only pure qutrit states are accessible by this method. To create a mixed state, some more complicated method is to be used. This method allows one to create arbitrary qutrit states and it implies a possibility to introduce controlled delay between three fundamental states forming the qutrit which could exceed the coherence length of the laser pump [13].

### D. Coherence matrix

We introduced only qualitative description of the qutrits based on biphotons so far. The quantitative measure characterizing the polarization properties of any single-mode state in the fourth moment in the field (including the biphoton state) was proposed by Klyshko [25]. It is a matrix consisting of six fourth-order moments of the electromagnetic field. An ordered set of such moments can be obtained using the direct product of $2\times 2$ coherence matrixes for both qubits. After normal ordering, averaging, and crossing out the redundant row and column the matrix takes the following form:

$$K_4 \equiv \begin{pmatrix} A & D & E \\ D^* & C & F \\ E^* & F^* & B \end{pmatrix}. \tag{11}$$

The diagonal elements are formed by real moments, which characterize the intensity correlation in two polarization modes $H$ and $V$:

$$A \equiv \langle \hat{a}^{\dagger 2}\hat{a}^2 \rangle, \quad B \equiv \langle \hat{b}^{\dagger 2}\hat{b}^2 \rangle, \quad C \equiv \langle \hat{a}^\dagger \hat{b}^\dagger \hat{a}\hat{b} \rangle. \tag{12}$$

Nondiagonal moments are complex:

$$D \equiv \langle \hat{a}^{\dagger 2}\hat{a}\hat{b} \rangle, \quad E \equiv \langle \hat{a}^{\dagger 2}\hat{b}^2 \rangle, \quad F \equiv \langle \hat{a}^\dagger \hat{b}^\dagger \hat{b}^2 \rangle. \tag{13}$$

Three real moments (12) and three complex ones (13) completely determine the state under consideration. The elements of the matrix (11) are expressed through the elements of the polarization density matrix. The normalization condition

$$A + B + 2C = 2 \tag{14}$$

reduces the number of independent real parameters, so for a mixed state we get eight parameters as expected. In the special case of a pure biphoton state, taking the average in Eqs. (12) and (13) over the state (2), we obtain the matrix components in the following form:

$$A = 2|c_1|^2, \quad B = 2|c_3|^2, \quad C = |c_2|^2. \tag{15}$$

$$D = \sqrt{2}c_1^* c_2, \quad E = 2c_1^* c_3, \quad F = \sqrt{2}c_2^* c_3. \tag{16}$$

So the links between the polarization density matrix and the matrix (11) can be found comparing the corresponding components of $(K_4)_{mk}$ and of $\underline{\rho \equiv |c\rangle\langle c|}$; $\rho_{mk} = c_m c_k^*; m,k = 1,2,3$ for a pure state and $\rho_{mk} = c_m c_k^*$ for a mixed state where the averaging, as usual, is taken over the classical probability distribution. The statistics of the field is assumed to be stationary and ergodic, so the time-averaged values of the observed quantities can be described in terms of a quantum statistical ensemble. In this case $\langle \cdots \rangle = \mathrm{Tr}(\rho \cdot \cdots)$, where $\rho$ is the polarization density operator.

## III. METHODS OF MEASUREMENT

What does it mean to measure the unknown state (2)? From the experimental point of view, it means that the experimentalist has to measure a complete set of real parameters (moments) determining the state. To do this the state must be subject to a set of unitary polarization transformations and projective measurements. By doing this one picks out the outcomes, which are proportional to the corresponding moments (12) and (13) or their linear combination. This procedure is known as quantum tomography. The quantum state can be represented using either the wave function, density matrix, or quasiprobability function (Wigner function). Probably the correct way to use the term "quantum tomography" is only for the reconstruction of the quasiprobability function because it gives the graphical representation of the state as a 3D plot. Nevertheless the term "quantum tomography" is also used for a general procedure of complete state reconstruction.

The methods of quantum tomography relate closely to the procedure of the classical tomography [26]. In [27] the technique of quantum tomography for the Wigner function based on the Radon transformation was suggested. A quantum-state reconstruction using the least-squares method was performed in [28]. The strategy of the maximal-likelihood method was suggested in Refs. [29,30]. Note that the maximal-likelihood method in the form which automatically recovers the density matrices for a physical state (a density matrix must be Hermitian, positive, and semidefinite and have the unity trace) was developed in [31,32]. For a brief review among the papers where this procedure was realized experimentally, let us mention Refs. [33–35] related to states defined by continuous variables. For states characterized by discrete variables, such as two polarization-spatial qubits, quantum tomography was realized in [18–21]. Recently quantum tomography has been performed for orbital angular momentum entangled qutrits [10], etc.

The physical idea behind the tomography procedure is performing measurements of appropriately complete set of observables called quorum [37] or just "looking" at the state from different positions. The minimal number of such positions might be the number of real parameters determining the state.

According to Bohr's complementarity principle, it is impossible to measure all moments (12) and (13) simultaneously, operating with a single qutrit only. So to perform a complete set of measurements one needs to generate a lot of representatives of a quantum ensemble.

First of all, let us mention that, at present, the only realistic way to register single-mode biphoton field is using the Brown-Twiss scheme. This scheme consists of a beam splitter followed by a pair of detectors connected with the coincidence circuit. It means that registration of a single biphoton, which carries the state (2), can give only a single event at the output of the experimental setup with some probability. So the statistical treatment of the outcomes becomes extremely important. For studying correlations between polarization degrees of freedom, which is essential in the case under consideration, the Brown-Twiss scheme must be accomplished with polarization filters introduced into each arm.

### A. Qutrit tomography protocols

We proposed two methods to perform polarization reconstruction of a biphoton qutrit state $|c_{in}\rangle$.

#### *1. Protocol 1*

The idea of the first method is splitting the state $|c_{in}\rangle$ into two spatial modes and performing transformations over two photons independently (Fig. 3). These transformations can be done using polarization filters placed in front of detectors. Each filter consists of a sequence of quarter- and half-wave plates and a polarization prism, which picks out definite linear polarization—for example, the vertical one. A narrowband filter centered at the doubled pump wavelength $\lambda = 2\lambda_p$ serves to make biphotons emitted from different sources indistinguishable in frequency as well as to reduce the background noise. An event is considered to be detected, if a pulse appears at the output of the coincidence circuit. Approximately in half of trials, one of the photons (signal, by convention) forming a biphoton is going to one of the detectors, while the other one (idler) is going to the other detector. In the remaining cases, both photons appear in the same output beam-splitter arm, and these events are not selected because they do not contribute to coincidences.

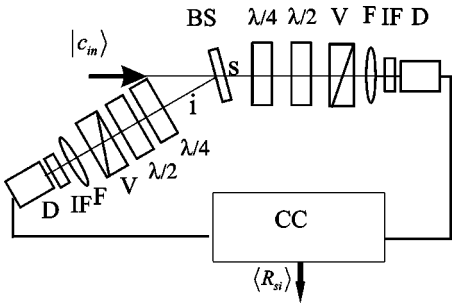


FIG. 3. Measurement block for protocol 1. The Brown-Twiss scheme for measuring intensity correlation between two polarization modes. After spatial separation at the nonpolarizing beam splitter (BS), signal ($s$) and idler ($i$) photons propagate through the quarter- and half wave plates, polarizing prisms (V), focusing lenses (F), and interference filters (IF) in two channels. Finally, photons are registered by detectors (D). The coincidence rate from the output of the coincidence circuit (CC) is proportional to the fourth moment in the field $\langle R_{si}\rangle$.

In the Heisenberg representation the polarization transformation for each beam-splitter output port is given by

$$\begin{pmatrix} a'^{\dagger} \\ b'^{\dagger} \end{pmatrix} = \begin{pmatrix} 0 & 0 \\ 0 & 1 \end{pmatrix} D_{\lambda/2}(\delta = \pi/2, \theta) \times D_{\lambda/4}(\delta = \pi/4, \chi) \times \begin{pmatrix} \frac{1}{\sqrt{2}} & 0 \\ 0 & \frac{1}{\sqrt{2}} \end{pmatrix} \begin{pmatrix} a^{\dagger} \\ b^{\dagger} \end{pmatrix}. \tag{17}$$

Four $2\times 2$ matrixes in the right-hand side of Eq. (17) describe the action of the nonpolarizing beam splitter, $\lambda/4$ and $\lambda/2$ plates, and vertical polarization prism on the state vector of the signal (idler) photon:

$$D_{\lambda/2,\lambda/4} = \begin{pmatrix} t & r \\ -r^* & t^* \end{pmatrix},$$

where $r$ and $t$ are the coefficients introduced in Eq. (8), so for a $\lambda/4$ plate ($\delta = \pi/4$),

$$t_{\lambda/4} = \frac{1}{\sqrt{2}}(1 + i\cos 2\chi), \quad r_{\lambda/4} = \frac{i}{\sqrt{2}}\sin 2\chi, \tag{18a}$$

and for a $\lambda/2$ plate ($\delta = \pi/2$),

$$t_{\lambda/2} = i\cos(2\theta), \quad r_{\lambda/2} = i\sin(2\theta). \tag{18b}$$

Thus, there are four real parameters (two for each channel) that determine polarization transformations. Namely, these parameters are orientation angles for two pairs of wave plates: $\theta_1, \chi_1, \theta_2, \chi_2$.

TABLE I. Protocol 1. Each line contains the orientation of the half- ($\theta_{s,i}$) and quarter- ($\chi_{s,i}$) wave plates in the measurement block. The last two columns show the corresponding moment $R_n$ and the process amplitude $M_v$ ($v=1,\ldots,9$).

| | Parameters of the experimental setup | | | | Moments to be measured | Amplitude of the process |
|---|---|---|---|---|---|---|
| $\nu$ | $\chi_s$ | $\theta_s$ | $\chi_i$ | $\theta_i$ | $R_{s,i}$ | $M_\nu$ |
| 1 | 0 | 45° | 0 | −45° | $A/4$ | $c_1/\sqrt{2}$ |
| 2 | 0 | 45° | 0 | 0 | $C/4$ | $c_2/2$ |
| 3 | 0 | 0 | 0 | 0 | $B/4$ | $c_3/\sqrt{2}$ |
| 4 | 45° | 0 | 0 | 0 | $\frac{1}{8}(B+C+2\ \mathrm{Im}\ F)$ | $\frac{1}{2\sqrt{2}}c_2-\frac{i}{2}c_3$ |
| 5 | 45° | 22.5° | 0 | 0 | $\frac{1}{8}(B+C-2\ \mathrm{Re}\ F)$ | $\frac{1}{2\sqrt{2}}c_2-\frac{1}{2}c_3$ |
| 6 | 45° | 22.5° | 0 | −45° | $\frac{1}{8}(A+C-2\ \mathrm{Re}\ D)$ | $\frac{1}{2}c_1-\frac{1}{2\sqrt{2}}c_2$ |
| 7 | 45° | 0 | 0 | −45° | $\frac{1}{8}(A+C+2\ \mathrm{Im}\ D)$ | $\frac{1}{2}c_1-\frac{i}{2\sqrt{2}}c_2$ |
| 8 | −45° | 11.25° | −45° | 11.25° | $\frac{1}{16}(A+B-2\ \mathrm{Im}\ E)$ | $\frac{1}{2\sqrt{2}}c_1+\frac{i}{2\sqrt{2}}c_3$ |
| 9 | 45° | 22.5° | −45° | 22.5° | $\frac{1}{16}(A+B-2\ \mathrm{Re}\ E)$ | $\frac{1}{2\sqrt{2}}c_1-\frac{1}{2\sqrt{2}}c_3$ |

As was mentioned above, the output of the Brown-Twiss scheme is the coincidence rate of the pulses coming from two detectors $D_s$ and $D_i$. The corresponding moment of the fourth order in the field has the following structure:

$$R_{s,i} \propto \langle b_s'^{\dagger} b_i'^{\dagger} b_s' b_i' \rangle = R(\theta_1, \chi_1, \theta_2, \chi_2). \tag{19}$$

In the most general case this moment contains a linear combination of six moments (12) and (13) forming the matrix $K_4$. So the main purpose of the quantum tomography procedure is extracting these six moments from the setup outcomes by varying the four parameters of the polarization Brown-Twiss scheme.

Consider some special examples, which give the corresponding lines in the complete protocol introduced below (Table I).

First of all, it is obvious that for measuring real moments (12) one needs to make polarization filters transmit both photons with horizontal polarizations to measure $A$, both photons with vertical polarization to measure $B$, and one photon with vertical and another one with horizontal polarizations to measure $C$. To do this all quarter-wave plates should be oriented at zero degrees, then to install both half-wave plates at zero degrees for measuring $B$; at $\theta_s=45°$ and $\theta_i=45°$ for measuring $A$; and at $\theta_s=0°$, $\theta_i=45°$ for measuring $C$. These settings pick out the squared modulus of corresponding amplitudes $c_3$, $c_1$, and $c_2$.

The next example shows how to measure one of the complex moments (13). To measure the real part of the moment $D$, let us set the wave plates in the Brown-Twiss scheme in the following way.

The idler channel:

$$\lambda/4:\ \chi_i = 0^\circ,\ D_{\lambda/4} = \frac{1}{\sqrt{2}}\begin{pmatrix} 1+i & 0 \\ 0 & 1-i \end{pmatrix};$$

$$\lambda/2:\ \theta_i = 45^\circ,\ D_{\lambda/2} = \begin{pmatrix} 0 & i \\ i & 0 \end{pmatrix}.$$

The signal channel:

$$\lambda/4:\ \chi_s = 45^\circ,\ D_{\lambda/4} = \frac{1}{\sqrt{2}}\begin{pmatrix} 1 & i \\ i & 1 \end{pmatrix};$$

$$\lambda/2:\ \theta_s = 22.5^\circ,\ D_{\lambda/2} = \frac{1}{\sqrt{2}}\begin{pmatrix} i & i \\ i & -i \end{pmatrix}.$$

Substituting these matrices into Eq. (17) and taking into account the commutation rules for the creation and annihilation operators it is easy to get the final moment to be measured:

$$R = \langle c | b_s^\dagger b_i^\dagger b_s b_i | c \rangle = \frac{1}{8}(A + C - 2\ \mathrm{Re}\ D).$$

A complete set of the measurements called the tomography protocol is presented in Table I. Each row corresponds to the setting of the plates to measure the moment placed in the sixth column. The last one corresponds to the amplitude of the process (see below).

This protocol was suggested and developed in [14–16]. A similar protocol was considered in detail earlier [36] for estimating the polarization state of a biphoton field, generated in a frequency-degenerate noncollinear mode. In this case the biphoton field is represented as a pair of polarization qubits.

Before describing the second method of state measurement let us make some remarks.

(i) We assume that the source generating qutrits is stationary. Since each measurement eliminates a qutrit, one has to be sure that there are a lot of copies of the initial state; each copy must be prepared in the same quantum state. Such an *ensemble approach* guarantees that the experimentalist deals with the same quantum state in all trials. In other words, the outcomes provide him with information about the same quantum state and elimination of a particular state does not affect the rest.

(ii) The outcomes of the setup are numbers related to the corresponding moments (19). Usually this number is the coincidence counting rate or the number of coincidences in a fixed time interval. Due to the necessity of a proper normalization of the state under investigation, the number of inde-

pendent real parameters grows up. The normalization is obtained from the measurement of moments $A$, $B$, and $C$. Furthermore, only the cosine and sine of the phases $\varphi_{12}$ and $\varphi_{13}$ can be measured in experiment as there is no way to measure the phases directly. That is why the final number of real parameters to be measured in experiment is 7 for a pure qutrit state and 9 for a mixed state.

(iii) To minimize the errors caused by independent statistical fluctuations of the outcomes, the number of moments (12) and (13) entering in Eq. (19) should be minimal.

#### *2. Protocol 2*

In the second method of quantum tomography, a biphoton qutrit being measured is first subject to a sequence of unitary transformations and, for each of such transformation, it is fed to the Brown-Twiss scheme settled for measuring a fixed moment. Using a wave plate with arbitrary optical thickness, one can achieve the quorum varying the orientation of the plate $\mu$.

In the most general case the coincidence counting rate in this protocol is a periodic function of $\mu$; moreover, its Fourier expansion contains nine harmonics of $\mu$: $\cos(0\mu)$, $\cos(2\mu)$, $\sin(2\mu)$, $\cos(4\mu)$, $\sin(4\mu)$, $\cos(6\mu)$, $\sin(6\mu)$, $\cos(8\mu)$, and $\sin(8\mu)$. These harmonics depend linearly on the nine moments $A$, $B$, $C$, Re $D$, Im $D$, Re $E$, Im $E$, Re $F$, and Im $F$. In other words, there is a $9\times 9$ matrix $T$ that links these nine harmonics to the nine moments as shown below:

$$\begin{pmatrix} \cos 0\mu \\ \cos 2\mu \\ \sin 2\mu \\ \cos 4\mu \\ \sin 4\mu \\ \cos 6\mu \\ \sin 6\mu \\ \cos 8\mu \\ \sin 8\mu \end{pmatrix} = T \begin{pmatrix} A \\ B \\ C \\ \mathrm{Re}\, F \\ \mathrm{Im}\, F \\ \mathrm{Re}\, D \\ \mathrm{Im}\, D \\ \mathrm{Re}\, E \\ \mathrm{Im}\, E \end{pmatrix}.$$

Unfortunately, the inverse matrix does not always exist. To simplify the problem we put only a single wave plate with fixed optical thickness ($\delta_s=\pi/2, \delta_i=\pi/4$) and fixed orientation $\chi_s, \theta_i$ in each channel of the Brown-Twiss scheme. In order to make sure the inverse matrix exists one needs to maximize the determinant of the matrix $T$ over the orientations of the plates $\chi_s, \theta_i$. After accomplishing this procedure we obtain $\chi_s \approx -28.5°$, $\theta_i \approx 19°$ (Fig. 4).

Instead of finding the links between the harmonics and moments, there is a more elegant method to reconstruct the quantum state using the second protocol (see Sec. III D). This method is considered in the present work.

### B. Experimental implementation: Protocol 1

The experimental setup for the quantum tomography of qutrits using protocol 1 is shown in Fig. 5. The *preparation block* includes a 2-mm BBO crystal with either type-I or type-II degenerate and collinear phase matching, which is pumped with cw argon laser operated at 351 nm wavelength. In the case of type-II phase matching, an additional quartz compensator is introduced right after the crystal. The state $\Psi_3=|0,2\rangle$ (for type I) or $\Psi_2=|1,1\rangle$ (for type II) generated in the crystal is fed to the *transformation block*. This block consists of the quartz plate with fixed optical thickness $\delta=0.9046$ and variable orientation $\alpha$. So the state, which is to be measured, is determined by the parameter $\alpha$. The *measurement block* is a Brown-Twiss scheme equipped with polarization filters placed in both arms (Fig. 3). Pulses coming from a couple of single-photon modules (EG&G SPCM-AQR) were fed to the counter through a standard time-to-amplitude converter.

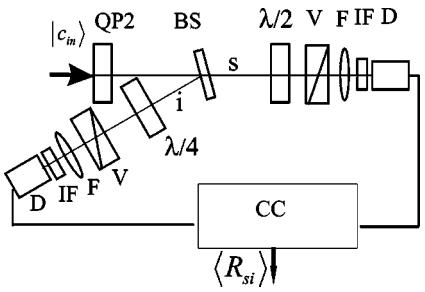


FIG. 4. Measurement block for protocol 2. An additional control quartz plate (QP2) serves as the state $|c_{in}\rangle$ tomography transformer. Only a single wave plate is introduced in each channel.

In our experiments the exposure time for measuring each moment is 5 sec. This time is an important experimental parameter. Each measurement consists of 30 runs, after which the scheme is reset. Namely each measurement is performed by setting the angles of wave plates $\chi_j$ and $\theta_j$ in both arms according to the tomographic protocol (Table I). After 30 runs, a new set of angles is selected and the next moment is measured in the same way. The output data of the setup are the mean coincidence counting rates. Examples of behavior for some moments ($A, B, C,$ Re $F,$ Im $F$) versus the orientation of the plate QP1 are plotted in Fig. 6.

### C. Experimental implementation: Protocol 2

For the second method we used Ti:Sa laser with pulse duration about 250 fsec, operating at 800 nm. After frequency doubling, the UV radiation with 400 nm wavelength was sent into the same setup as described above. For this protocol we used 2-mm BBO crystal cut for collinear degen-

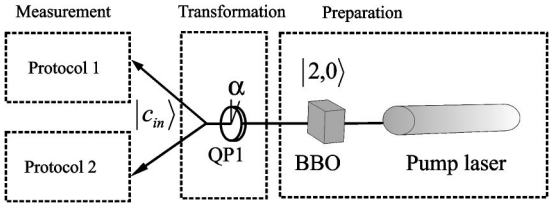


FIG. 5. Scheme of qutrits tomograph, consisting of three blocks. Preparation block includes pump laser(s) and nonlinear crystal(s). Transformation block is the quartz plate (QP1) which orientation angle $\alpha$ determines the final state to be measured. The measurement block depends on the protocol to be used (see Figs. 3 and 4).

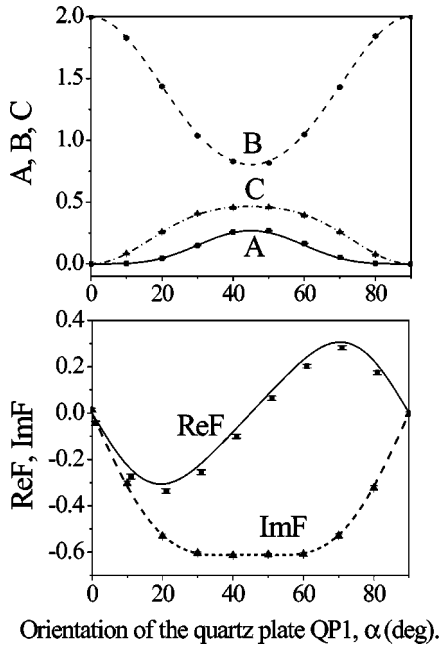


FIG. 6. Some components of the matrix $K_4$ versus the orientation of the quartz plate QP1. Different angles of the plate correspond to different states sent to the measurement block. The plot at the top corresponds to measured real moments $A$ (squares), $B$ (circles), and $C$ (triangles) and theoretical predictions $A(--)$, $B(--)$, and $C(-\circ-)$. The plot at the bottom shows measured complex moment Re $F$ (squares) and Im $F$ (triangles), and theoretical predictions Re $F$ (short-dashed line) and Im $F$ (long-dashed line).

erate type-I phase matching. A quartz plate with the optical thickness $\delta=0.656$ is placed after the BBO crystal to prepare the qutrit state to be measured. The measurement part of the setup was slightly changed (Fig. 4). An additional control quartz plate introduced in front of the beam splitter accomplishes the protocol. Its orientation angle $\mu$ is a parameter defining the measurement process. The control plate is rotated with 5° steps from 0 up to 360° so that protocol 2 consists of 72 measurements. Each arm of the Brown-Twiss scheme contains either a quarter- or half-wave plate with fixed orientation. The orientations are $\chi_1=18.8°$ for the quarter-wave plate in the first channel and $\theta_2=-28.5°$ for the half-wave plate in the second channel. Protocol 2 is easier to implement since only a single parameter $\mu$ is changed whereas four $\chi_{1,2}, \theta_{1,2}$ parameters are varied in protocol 1. In perspective, this kind of protocol allows one to automate the quantum tomography procedure: the control plate can be rotated continuously and reconstruction of the quantum state can be based on analysis of coincidence rates corresponding to the respective values of $\mu_i$ $(i=1,\ldots,72)$.

### D. Statistical reconstruction of biphoton-field qutrits from the outcomes of mutually complementary measurements

Each of the nine processes from protocol 1 as well as of the 72 processes from protocol 2 is described by its amplitude $M_\nu$. From the statistical point of view, the squared modulus of the process amplitude specifies the intensity of the event generation:

$$R_\nu = M_\nu^* M_\nu. \tag{20}$$

The considered processes are examples of mutually complementary sets of measurements in the sense of Bohr's complementarity principle. The event-generation intensities $R_\nu$ for both protocols are the main quantities accessible from the measurement. Making the bridge between statistical and physical description of the process the quantities $R_\nu$ coincide with the fourth moments in the field introduced above in Eq. (19). Their dimension is the frequency unit (Hz). The number of events occurring within any given time interval obeys the Poisson distribution. Therefore, the quantities $R_\nu$ specify the intensities of the corresponding mutually complementary Poisson processes and serve as estimates of the Poisson parameters $\lambda_\nu$ (see below).

Although the amplitudes of the processes cannot be measured directly, they are of the greatest interest as these quantities describe fundamental relationships in quantum physics. It follows from the superposition principle that the amplitudes are linearly related to the state-vector components. So the main purpose of quantum tomography is the reproduction of the amplitudes and state vectors, which are hidden from direct observation.

The linear transformation of the state vector $c=\{c_1,c_2,c_3\}$ into the amplitude of the process $M$ is described by a certain matrix $X$. For example, considering the first protocol this matrix can be easily obtained from Table I (last column in Table I):

$$X = \begin{pmatrix} 1/\sqrt{2} & 0 & 0 \\ 0 & 1/2 & 0 \\ 0 & 0 & 1/\sqrt{2} \\ 0 & 1/(2\sqrt{2}) & -i/2 \\ 0 & 1/(2\sqrt{2}) & -1/2 \\ 1/2 & -1/(2\sqrt{2}) & 0 \\ 1/2 & -i/(2\sqrt{2}) & 0 \\ 1/(2\sqrt{2}) & 0 & i/(2\sqrt{2}) \\ 1/(2\sqrt{2}) & 0 & -1/(2\sqrt{2}) \end{pmatrix}. \tag{21}$$

Using the matrix $X$ the complete set of nine amplitudes of the processes can be expressed by a single equation

$$Xc = M. \tag{22}$$

The matrix $X$ is an instrumental matrix for a set of mutually complementary measurements, by analogy with the conventional instrumental function. The implementation of the method to the first protocol has been considered in [15].

Consider an algorithm allowing one to calculate the instrumental matrix $X$ for protocol 2. The matrix consists of 72 rows (the number of control plate orientations) and 3 columns (the dimension of Hilbert space for qutrits). Each row is formed in the following way. Using the coefficients the $t^{(s,i)}$ and $r^{(s,i)}$ of the wave plates introduced to the signal and idler channels of the Brown-Twiss scheme (18a) and (18b) the three-element row, which defines the process amplitude right after the control plate, can be written in the form

$$l = \left[ r^{(s)}_{\lambda/2} r^{(i)}_{\lambda/4} \quad \frac{1}{\sqrt{2}} (r^{(s)}_{\lambda/2} t^{(i)}_{\lambda/4} + r^{(i)}_{\lambda/4} t^{(s)}_{\lambda/2}) \quad t^{(s)}_{\lambda/2} t^{(i)}_{\lambda/4} \right]. \quad (23)$$

The unitary matrix $G$ is defined by the control plate according to Eqs. (7) and (8), with a replacement $\alpha \rightarrow \mu$, where $\mu$ is the control plate orientation (it takes 72 values from 0° to 355°). We chose the control plate to be a quarter-wave plate, so $\delta = \pi/4$. Finally,

$$G = G(\mu_i), \quad i = 1,2, \ldots, 72. \quad (24)$$

Each row of the instrumental matrix $X$ (72 rows, 3 columns) is defined by the product of the row $l$ (which is the same for any process) and the matrix $G$ (which is defined by the control plate orientation angle):

$$X_i = lG(\mu_i), \quad i = 1,2, \ldots, 72, \quad (25)$$

where $X_i$ is the $i$th row of the matrix $X$.

## IV. METHODS OF QUANTUM-STATE RECONSTRUCTION

In the simplest case the density matrix can be estimated directly from the measurements. Since the set of experimental data is limited in this case, the reconstructed density matrix may have nonphysical properties like negative eigenvalues. But in the general case of $s$-dimensional systems the problem of density matrix reconstruction using the direct results of measurements cannot be solved since the corresponding inverse problem is ill posed.

When analyzing the experimental data, we use the so-called root estimator of quantum states [17]. This approach is designed specially for the analysis of mutually complementary measurements (in the sense of Bohr's complementarity principle). The advantage of this approach consists of the possibility of reconstructing states in a high-dimensional Hilbert space and reaching the accuracy of reconstruction of an unknown quantum state close to its fundamental limit. Below we consider two methods of quantum-state root estimation that give similar results. They are the least-squares method (LSM) and maximum-likelihood method (MLM).

### A. Least-squares method

In statistical terms, Eq. (22) is a linear regression equation. A distinctive feature of the problem is that only the absolute value of the process amplitude $M$ is measured in the experiment. The estimate of the absolute value of the amplitude is given by the square root of the corresponding experimentally measured coincidence rate:

$$|M_\nu|^{\text{expt}} = \sqrt{k_\nu / t}, \quad (26)$$

where $k_\nu$ is the number of events (coincidences) detected in the $\nu$th process during the measurement time $t$.

It is worth noting that, by the action of the root-square procedure on a Poissonian random value, one gets the random variable with a uniform variance—i.e., at the variance stabilization [38]. Note also, since we do not deal with event probabilities but with their rates or intensities, it is convenient to use un-normalized state vectors. These vectors allow the coincidence counting rate (event-generation intensities) to be derived directly from Eqs. (20) and (22) without introducing coefficients related to the biphoton generation rate, detector efficiencies, etc. The dimensionality of the vector state obtained in such a way is $1/\sqrt{\text{time}}$. The final state vector obtained by the reconstruction procedure, nevertheless, should be normalized to unity.

Assuming that the variances of different $|M_\nu|^{\text{expt}}$ are independent and identical, one can apply the standard least-squares estimate to Eq. (22) [39]:

$$c = (X^\dagger X)^{-1} X^\dagger M. \quad (27)$$

Unlike the traditional least-squares method, Eq. (27) cannot be used for an explicit estimation of the state vector $c$, because it is to be solved by the iteration method. The absolute value of $M$ is known from the experiment ($|M_\nu| = |M_\nu|^{\text{expt}}$). We assume that the phase of vector $Xc$ at the $i$th iteration step determines the phase of the vector $M$ at the $(i+1)$th step. In other words, the phase is determined by the iteration procedure.

It turns out that, for the Gaussian approximation of Poisson's quantities, this least-squares estimate coincides with a more exact and rigorous maximum-likelihood estimate considered below.

### B. Maximum-likelihood method

The likelihood function is defined by the product of Poissonian probabilities:

$$L = \prod_i \frac{(\lambda_i t_i)^{k_i}}{k_i!} e^{-\lambda_i t_i}, \quad (28)$$

where $k_i$ is the number of coincidences observed in the $i$th process during the measurement time $t_i$, and $\lambda_i$ are the unknown theoretical event-generation intensities (expected number of coincidences proportional to the moments in the field), whose estimation is the subject of this section.

The logarithm of the likelihood function is, if we omit an insignificant constant,

$$\ln L = \sum_i [k_i \ln(\lambda_i t_i) - \lambda_i t_i]. \quad (29)$$

Let us introduce the matrices with the elements defined by the following formulas:

$$I_{js} = \sum_i t_i X^*_{ij} X_{is}, \quad (30)$$

$$J_{js} = \sum_i \frac{k_i}{\lambda_i} X^*_{ij} X_{is}, \quad j,s = 1,2,3. \quad (31)$$

The matrix $I$ is determined from the experimental protocol and, thus, is known *a priori* (before the experiment). This is the Hermitian matrix of Fisher's information. The matrix $J$ is determined by the experimental values of $k_i$ and by the unknown event-generation intensities $\lambda_i$. This is the empirical matrix of Fisher's information (see also the Appendix).

In terms of these matrices, the condition for the extremum of the function (29) can be written as

TABLE II. Results of the state reconstruction. The left column indicates the orientation of the quartz plate QP1, determining the state to be measured. Values of the optical thickness of QP1 are $\delta=0.656$ for the pulsed regime (protocols 1 and 2) and $\delta=0.9046$ for the cw regime (protocol 1). Theoretical state vectors are placed in the right column. The table contains the amplitudes of the reconstructed states $(c_1, c_2, c_3)$ as well as their fidelities, calculated by least-squares (LSM) and maximum-likelihood (MLM) methods.

| | | | Pulsed regime, $\delta=0.656$, protocol 1 | | |
|---|---|---|---|---|---|
| $\alpha$ | Fidelity | | State vector: experiment | | State vector: theory |
| | LSM | MLM | LSM | MLM | $(c_1, c_2, c_3)_{theory}$ |
| 0° | 0.99981 | 0.99979 | $-0.0046+0.0040i$ | $-0.0065+0.0057i$ | 0 |
| | | | $-0.0050-0.0115i$ | $-0.0053-0.0102i$ | 0 |
| | | | 0.9999 | 0.9999 | 1 |
| 40° | 0.9989 | 0.9989 | $-0.3669-0.0691i$ | $-0.3669-0.0687i$ | $-0.3482-0.0948i$ |
| | | | $-0.0657+0.6814i$ | $-0.0653+0.6815i$ | $-0.0900+0.6732i$ |
| | | | 0.6261 | 0.6261 | 0.6392 |
| 80° | 0.9993 | 0.9993 | $-0.0088+0.0439i$ | $-0.0091+0.0439i$ | $-0.0136+0.0413i$ |
| | | | $0.1691+0.2587i$ | $0.1697+0.259i$ | $0.1691+0.2338i$ |
| | | | 0.9500 | 0.9498 | 0.9565 |
| | | | Pulsed regime, $\delta=0.656$, protocol 2 | | |
| 0° | 0.99846 | 0.99847 | $-0.0071-0.0135i$ | $-0.0072-0.0135i$ | 0 |
| | | | $0.0359+0.0046i$ | $0.0357+0.0046i$ | 0 |
| | | | 0.9992 | 0.9992 | 1 |
| 40° | 0.9991 | 0.9991 | $-0.3442-0.1139i$ | $-0.3444-0.1142i$ | $-0.3482-0.0948i$ |
| | | | $-0.0987+0.6546i$ | $-0.0990+0.6545i$ | $-0.0900+0.6732i$ |
| | | | 0.6560 | 0.6559 | 0.6392 |
| 80° | 0.9981 | 0.9981 | $-0.0093+0.0430i$ | $-0.0094+0.0430i$ | $-0.0136+0.0413i$ |
| | | | $0.2122+0.2408i$ | $0.2121+0.2408i$ | $0.1691+0.2338i$ |
| | | | 0.9461 | 0.9461 | 0.9565 |
| | | | cw regime, $\delta=0.9046$, protocol 1 | | |
| 0° | 0.99325 | 0.99313 | $-0.0030-0.0512i$ | $-0.0028-0.0514i$ | 0 |
| | | | 0.9966 | 0.9966 | 1 |
| | | | $-0.0015-0.0642i$ | $-0.0013-0.0649i$ | 0 |
| 60° | 0.9886 | 0.9799 | 0.7236 | 0.7244 | 0.7052 |
| | | | $0.1165-0.1231i$ | $0.1245-0.1210i$ | $0.0392-0.0616i$ |
| | | | $0.2792+0.6080i$ | $0.1694+0.6453i$ | $0.2990+0.6387i$ |

$$Ic = Jc. \tag{32}$$

Hence, it follows that

$$I^{-1}Jc = c. \tag{33}$$

The latest relationship is known as the likelihood equation. This is a nonlinear equation, because $\lambda_i$ depends on the unknown state vector $c$. Because of the simple quasilinear structure, this equation can easily be solved by the iteration method [17]. The quasi-identity operator $I^{-1}J$ acts as the identical operator upon only a single vector in the Hilbert space—namely, on the vector corresponding to the solution of Eq. (33) and representing the maximum possible likelihood estimate for the state vector. The condition for the existence of the matrix $I^{-1}$ is a condition imposed on the initial experimental protocol. The resulting set of equations automatically includes the normalization condition, which is written as

$$\sum_i k_i = \sum_i (\lambda_i t_i). \tag{34}$$

This condition implies that, for all processes, the total number of detected events is equal to the sum of the products of event detection frequencies during the measurement time.

### C. Analysis of the experimental data

#### *1. Pure-state reconstruction*

The examples of qutrit state reconstruction using both the least-squares and maximum-likelihood methods are given in Table II.

The value of the fidelity parameter $F$ is defined as

$$F = |\langle c_{theory}|c_{\text{expt}}\rangle|^2. \tag{35}$$

It gives a conventional measure of the correspondence between the theoretical and experimental state vectors.

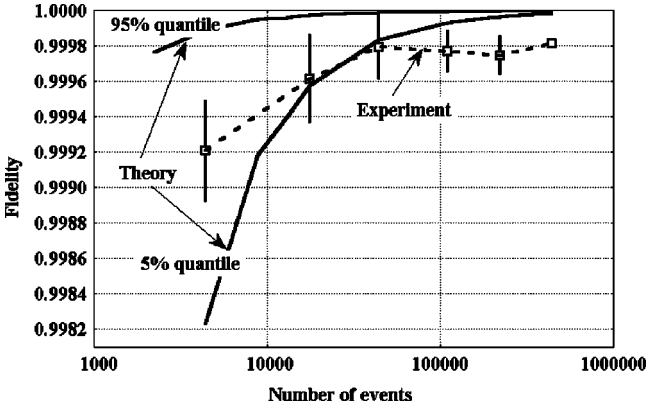


FIG. 7. Fidelity dependence on the sample size. Mean values and standard deviations corresponding to the sample volumes $f=0.01,0.04,0.1,0.25,0.5,1.0$.

The dependence of fidelity on the amount of experimental data obtained is shown in Fig. 7. This figure shows the fidelity achieved in the experiment in comparison with the theoretical range (see the Appendix for more details). The lower boundary corresponds to 5% quantile of statistical distribution, while the upper to 95% quantile. It is clearly seen that the fidelity value achieved experimentally for a small volume of experimental data is completely within the limits of the theoretical range, while it goes out for a higher volume. Such behavior of fidelity is due to the existence of two different error types arising under the reconstruction of quantum states. Let us call them statistical and instrumental errors, respectively. The statistical errors are caused by a finite number of quantum system representatives to be measured. As the measurement time increases, the information about the quantum state of interest progressively increases (see the Appendix). Accordingly, the statistical error becomes smaller. The instrumental errors are caused by the researcher's incomplete knowledge of the system; i.e., more exact information exists, in principle, but it is inaccessible to the experimenter. Thus, a comparison between the state reconstruction result and the fundamental statistical level of accuracy can serve as a guide for the parameter adjustment of the setup.

Thus, for a small volume of experimental data, statistical errors prevail, whereas for large sample sizes, the setting errors and the instability of protocol parameters dominate. The number of events at which the statistical error becomes smaller than the instrumental error can be called the coherence volume. Numerically the coherence volume can be estimated as the intersection point between the experimental fidelity and the lower theoretical fidelity curve. In our case this value is about 25 000–30 000 events. Starting approximately from this value, fidelity is reaching saturation and further growth of experimental data volume does not lead to an increase in the precision of quantum system estimation.

Figure 7 relates to the state defined by the orientation angle of the quartz plate QP1 $\alpha=50°$ (for protocol 2). To plot Fig. 7 we used the following technique for passing from full-volume experiment to a partial-volume experiment. Let us consider the parameter $0<f\leqslant 1$, which characterizes the volume of experimental data. Suppose that $f=1$ for a full-volume experiment. A partial-volume experiment may be introduced considering the observation time $t'_\nu=ft_\nu$ instead of $t_\nu$. Hence, performing a single full-volume experiment means providing with a large (practically infinite) number of partial-volume experiments.

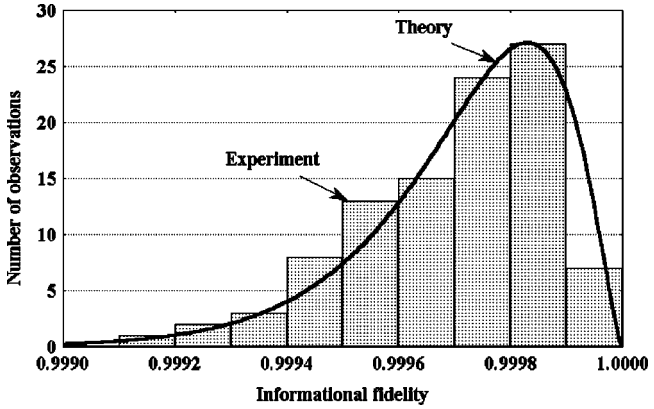


FIG. 8. Informational $\chi^2$ criterion for small sample sizes: sample size=4400.

For a given volume of experimental data $f$ each event from the full-volume experiment is picked up with the probability $f$ and rejected with the probability $1-f$. Due to the presence of statistical fluctuations, the equation for the number of observations, $k_\nu(t'_\nu)=fk_\nu(t_\nu)$, is violated. Therefore a unique estimate of the state vector corresponds to every partial-volume experiment. Figure 7 shows mean values and standard deviations corresponding to volumes $f=0.01,0.04,0.1,0.25,0.5,1.0$. For each $f<1$, ten experiments were simulated.

The results of informational fidelity research, introduced in the Appendix, are shown in Figs. 8 and 9. These figures correspond to the same data set as shown in Fig. 7. The distribution density of informational fidelity for a small (compared to the coherence volume) sample size closely agrees with the theoretical result given by Eq. (A14) (see Fig. 8). In this case the instrumental error is negligibly small compared to the statistical one. When the sample volume is close to the coherence volume (Fig. 9) the influence of instrumental and statistical errors is about equal. In other

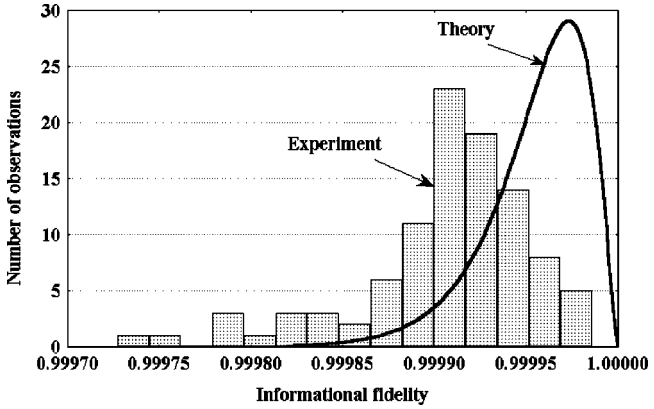


FIG. 9. Informational $\chi^2$ criterion for large sample sizes: sample size=27 750. The disagreement between observations and theoretical curve for large sample sizes is due to the instrumental error.

TABLE III. Example of the mixture separation using quasi-Bayesian algorithm for the given state. cw regime, protocol 1.

| State vector: theory | Density matrix: experiment | |
|---|---|---|
| | First principal component | Second principal component |
| $\alpha=30°$ | weight=0.9238 | weight=0.0762 |
| $\delta=0.9046$ | $(c_1,c_2,c_3)^1_{expt}$ | $(c_1,c_2,c_3)^2_{expt}$ |
| $(c_1,c_2,c_3)_{theory}$ | | |
| 0.7052 | 0.7019 | $-0.3027-0.2858i$ |
| $-0.0392-0.0616i$ | $-0.0466-0.1325i$ | $-0.6529+0.3291i$ |
| $0.2990-0.6387i$ | $0.2245-0.6612i$ | $0.5140-0.1668i$ |
| | Fidelity=0.9916 | |

words, the informational losses caused by averaging over instrumental errors are approximately equal to the losses caused by statistical ones. Finally, if the sample size is greater than the coherence volume, instrumental errors predominate. It means that the statistical informational errors are negligibly small compared to the instrumental ones.

#### *2. Mixture separation algorithm*

Let us describe the algorithm for reconstructing a two-component mixed state. This algorithm can be easily generalized to an arbitrary number of components.

The total number of events observed in every process is divided between the components proportional to the intensity:

$$k_\nu^{(1)} = k_\nu \frac{\lambda_\nu^{(1)}}{\lambda_\nu^{(1)}+\lambda_\nu^{(2)}}, \quad k_\nu^{(2)} = k_\nu \frac{\lambda_\nu^{(2)}}{\lambda_\nu^{(1)}+\lambda_\nu^{(2)}}, \tag{36}$$

where $\nu=1,2,\ldots,\nu_{max}$ and $\nu_{max}$ is the total number of processes; $\lambda_\nu^{(1)}$ and $\lambda_\nu^{(2)}$ are the estimates of intensities of processes for a given step of the iteration procedure.

At a certain iteration step, let us represent $k_\nu$ as a sum of two components:

$$k_\nu = k_\nu^{(1)} + k_\nu^{(2)}. \tag{37}$$

For each component, we can obtain the estimates for the state vector, amplitudes, and intensity of the processes according to the method of pure-state analysis described in the previous section. Since we get new intensity estimates, let us again split the total number of events in every process proportionally to the intensities of the components. In such a way, a new iteration is formed and the whole procedure is repeated. The described process is called quasi-Bayesian algorithm [17].

As a result, the iteration process converges to some (nonnormalized) components $c^{(1)}$ and $c^{(2)}$. Thus, the mixture separation algorithm reduces to numerous estimations of pure components according to the simple algorithm described above in Sec. IV B. As a result of the whole algorithm execution, the estimate for the density matrix of the mixture appears:

$$\rho = c^{(1)}c^{(1)\dagger} + c^{(2)}c^{(2)\dagger}, \tag{38}$$

TABLE IV. Analysis of the principal components of the density matrix for the state (41) and (42): numerical simulation.

| State vector $(c_1,c_2,c_3)$ | | Fidelity |
|---|---|---|
| First principal component | | |
| Experiment weight =0.6188 | Theory weight =0.6143 | |
| $-0.3658-0.0448i$ | $-0.3668-0.0211i$ | 0.9985 |
| $0.2085+0.4743i$ | $0.2294+0.4934i$ | |
| 0.7718 | 0.7543 | |
| Second principal component | | |
| Experiment weight=0.3812 | Theory weight=0.3857 | |
| $-0.1208-0.2643i$ | $-0.1490-0.2382i$ | 0.9979 |
| $-0.1659-0.8150i$ | $-0.1986-0.7942i$ | |
| 0.4731 | 0.5009 | |

$$\rho \to \frac{\rho}{\mathrm{Tr}(\rho)}. \tag{39}$$

The last procedure is normalization of the density matrix.

A remarkable feature of the algorithm is that according to numerical calculations, independent of zero-approximation selection of the mixture components, the resulting density matrix $\rho$ is always the same. Of course, the components $c^{(1)}$ and $c^{(2)}$ are different for the random selection of the zero approximation.

The mixed-state reconstruction accuracy is described by the following fidelity:

$$F = \left[\mathrm{Tr}\sqrt{\sqrt{\rho^{(0)}}\rho\sqrt{\rho^{(0)}}}\right]^2, \tag{40}$$

where $\rho^{(0)}$ and $\rho$ are the exact and reconstructed density matrices, respectively. For a pure state $[\rho^2=\rho,(\rho^{(0)})^2=\rho^{(0)}]$ fidelity (40) converts to Eq. (35).

Actually in the present work we did not intend to generate a given mixed state of qutrits in experiment; it will be done later [40]. Nevertheless, applying the described algorithm to the data we can check whether the state produced in our system is pure. For example, consider the case when the state $\Psi_2=|1,1\rangle$ is fed to the quartz plate QP1 (see Table II). This state is the most interesting to be tested, since $|H,V\rangle$ and $|V,H\rangle$ are distinguishable due to the polarization dispersion in BBO crystal. Namely, extraordinarily polarized photons ($H$) propagate faster than ordinary ($V$) ones in the crystal. Therefore a group velocity compensator has to be used for making them indistinguishable [41]. Nonperfect compensation (we reached 95% visibility for polarization interference) is the main reason why the fidelity reconstruction for these states is not so high. The results of applying quasi-Bayesian algorithm to the reconstructed state are in Table III. We chose the state corresponding to the angle $\alpha=30°$. It is clearly seen that the weight of the first principal component is much greater than that of the second one. Doing the same procedure with the $\Psi_1=|2,0\rangle$ initial state, we have checked that the estimator for a pure-state vector is extremely close to the estimator of the major density matrix component.

To illustrate the quasi-Bayesian approach, let us consider a result of reconstruction for a two-component mixture using protocol 1. Suppose one has a mixture of two pure states prepared from $|2,0\rangle$ by quartz plates QP1′ and QP1″ oriented at angles $\alpha=-30°$ and $\alpha=50°$, respectively. Let the optical thickness of both plates be $\delta=0.656$. Ten thousand events were generated (on the average) for every component. The theoretical density matrix for the mixed state under consideration is

$$\rho^{(0)}=\begin{pmatrix} 0.1134 & 0.0263+0.0808i & -0.1987-0.0558i \\ 0.0263-0.0808i & 0.4404 & 0.0679+0.0752i \\ -0.1987+0.0558i & 0.0679-0.0752i & 0.4462 \end{pmatrix}. \tag{41}$$

A typical example of a reconstructed density matrix is the following:

$$\rho=\begin{pmatrix} 0.1162 & 0.0294+0.0808i & -0.1965-0.0691i \\ 0.0204-0.0808i & 0.4298 & 0.0697+0.0796i \\ -0.1965+0.0691i & 0.0697-0.0796i & 0.4540 \end{pmatrix}. \tag{42}$$

The reconstructed matrix fidelity is $F=0.999\,431$. An analysis of the principal components of density matrix is given in Table IV.

This example shows a reasonably high accuracy of mixed-state reconstruction. The statistical properties of the proposed algorithm were studied by means of the Monte Carlo method. One hundred numerical experiments were conducted similar to the one described above. To verify the reliability, the solution was found twice for each experiment (with random zero-approximation selection). The solutions appeared to be equal for all cases (within a negligibly small computational error). The obtained statistical fidelity distribution is shown in Fig. 10. Numerical research shows that the fidelity distribution density is well described by the $\beta$ distribution.

## V. CONCLUSION

The procedure of quantum-state measurement for a three-state optical system formed by a frequency and spatially degenerate two-photon field has been considered in this work. A method of statistical estimation of the quantum state through solving the likelihood equation and examining the statistical properties of the resulting estimates has been developed. Based on the experimental data (fourth-order moments in the field) and the root method of estimating quantum states, the initial wave function of qutrits has been reconstructed.

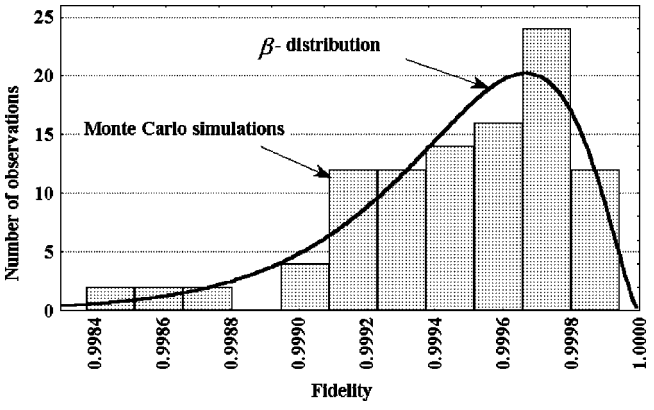


FIG. 10. Simulation of the fidelity between theoretical and reconstructed density matrices in a mixture separation problem. Here 100 numerical experiments of 20 000 events per each (on the average) were made.

Experimental data analysis is based on representing the event-generation intensity for each one of mutually complementary quantum processes as a squared module of some amplitude. A complete set of measured processes amplitudes can be compactly described using the instrumental matrix. In the framework of the formalism of a process amplitude one can apply effective tools for the quantum state reconstruction: least-squares and maximum-likelihood methods.

The developed analysis tools provide the means of quantum-state reconstruction from the experimental data with high accuracy and reliability. The estimate accuracy is determined by the concurrence of two types of errors: statistical ones and instrumental ones. For smaller sample sizes statistical errors are dominant, while for greater ones instrumental errors dominate.

Instrumental errors lead to fidelity saturation at less than unity level. In the present work, fidelity for most of performed experiments (more than 20) exceeded a level of 0.995. For many cases the level of 0.9998 was achieved.

## ACKNOWLEDGMENTS

Useful discussions with A. Burlakov, A. Ekert, B. Englert, D. Kazlikowski, and A. Lamas-Linares are gratefully acknowledged. This work was supported in part by the Russian Foundation of Basic Research (Project Nos. 03-02-16444 and 02-02-16843), National University of Singapore Program WBS (Project No. R-144-000-100-425), and the National University of Singapore's Eastern Europe Research Scientist and Student Programme. One of us (L.K.) acknowledges support from a INTAS-YS grant (No. 03-55-1971).

## APPENDIX: STATISTICAL FLUCTUATIONS OF THE STATE VECTOR

As was already mentioned above, an un-normalized state vector provides the most complete information about a quantum system. The use of an un-normalized vector allows us to remove an interaction constant in Eq. (22). The norm of the vector $c$, obtained as a result of quantum system reconstruction, provides one with information about the total intensity of all the processes considered in the experiment. However, the fluctuations of the quantum state (and norm fluctuations, in particular) in a normally functioning quantum information system should be within a certain range defined by the statistical theory. The present section is devoted to this problem.

The practical significance of accounting for statistical fluctuations in a quantum system relates to developing methods of estimation and control of the precision and stability of a quantum information system evolution, as well as methods of detecting external interception (Eve's attack on the quantum channel between Alice and Bob).

The estimate of the un-normalized state vector $c$, obtained by the maximum-likelihood principle, differs from the exact state vector $c^{(0)}$ by the random values $\delta c = c^{(0)} - c$. Let us consider the statistical properties of the fluctuation vector $\delta c$ by expansion of the log-likelihood function near a stationary point:

$$\delta \ln L = -\left[\frac{1}{2}(K_{sj}\delta c_s \delta c_j + K_{sj}^{*}\delta c_s^{*}\delta c_j^{*}) + I_{sj}\delta c_s^{*}\delta c_j\right]. \tag{A1}$$

Together with the Hermitian matrix of the Fisher information $I$, Eq. (30), we define the symmetric Fisher information matrix $K$, whose elements are defined by the following equation:

$$K_{sj} = \sum_{\nu} \frac{k_\nu}{M_\nu^2} X_{\nu s} X_{\nu j}, \tag{A2}$$

where $M_\nu$ is the amplitude of the $\nu$th process. In the general case, $K$ is a complex symmetric non-Hermitian matrix. From all possible types of fluctuations, let us pick out the so-called gauge fluctuations. Infinitesimal global gauge transformations of a state vector are as follows:

$$\delta c_j = i\varepsilon c_j, \quad j = 1,2,\ldots,s, \tag{A3}$$

where $\varepsilon$ is an arbitrary small real number and $s$ is the Hilbert space dimension.

Evidently, for gauge transformations, $\delta \ln L = 0$. It means that two state vectors that differ by a gauge transformation are statistically equivalent; i.e., they have the same likelihood. Such vectors are physically equivalent since the global phase of the state vector is nonobservable. From a statistical point of view, the set of mutually complementing measurements should be chosen in such a way that for all other fluctuations (except gauge fluctuations) $\delta \ln L < 0$. This inequality serves as the statistical completeness condition for the set of mutually complementing measurements.

Let us derive some constructive criteria of the statistical completeness of measurements. The complex fluctuation vector $\delta c$ is conveniently represented by a real vector of double length. After extracting the real and imaginary parts of the fluctuation vector $\delta c_j = \delta c_j^{(1)} + i\,\delta c_j^{(2)}$ we transfer from the complex vector $\delta c$ to the real one $\delta\xi$:

$$\delta c = \begin{pmatrix} \delta c_1 \\ \vdots \\ \delta c_s \end{pmatrix} \rightarrow \delta\xi = \begin{pmatrix} \delta c_1^{(1)} \\ \vdots \\ \delta c_s^{(1)} \\ \delta c_1^{(2)} \\ \vdots \\ \delta c_s^{(2)} \end{pmatrix}. \tag{A4}$$

In the particular case of qutrits ($s=3$) this transition provides us with a six-component real vector instead of a three-component complex vector.

In the new representation, Eq. (A1), becomes

$$\delta \ln L = -H_{sj}\delta\xi_s\delta\xi_j = -\langle \delta\xi | H | \delta\xi \rangle, \tag{A5}$$

where matrix $H$ is the "complete information matrix" possessing the following block form:

$$H = \begin{pmatrix} \mathrm{Re}(I+K) & -\mathrm{Im}(I+K) \\ \mathrm{Im}(I-K) & \mathrm{Re}(I-K) \end{pmatrix}. \tag{A6}$$

The matrix $H$ is real and symmetric. It is of double dimension, respectively, to the matrices $I$ and $K$. For qutrits, $I$ and $K$ are $3\times 3$ matrices, while $H$ is $6\times 6$.

Using matrix $H$ it is easy to formulate the desired characteristic completeness condition for a mutually complementing set of measurements. For a set of measurements to be statistically complete, it is necessary and sufficient that one and only one eigenvalue of the complete information matrix $H$ is equal to zero, while the other ones are strictly positive.

We would like to stress that checking the condition one not only verifies the statistical completeness of a measurement protocol, but also ensures that the obtained extremum is of maximum likelihood.

An eigenvector that has eigenvalue equal to zero corresponds to gauge fluctuation direction. Such fluctuations do not have a physical meaning as stated above. Eigenvectors corresponding to the other eigenvalues specify the direction of fluctuations in the Hilbert space.

The principal fluctuation variance is

$$\sigma_j^2 = \frac{1}{2h_j}, \quad j = 1,\ldots,2s-1, \tag{A7}$$

where $h_j$ is the eigenvalue of the information matrix $H$, corresponding to the $j$th principal direction.

The most critical direction in the Hilbert space is the one with the maximum variance $\sigma_j^2$, while the corresponding eigenvalue $h_j$ is accordingly minimal. Knowledge of the numerical dependence of statistical fluctuations allows one to estimate distributions of various statistical characteristics.

The important information criterion that specifies the general possible level of statistical fluctuations in a quantum information system is the $\chi^2$ criterion. It can be expressed as

$$2\langle \delta\xi|H|\delta\xi\rangle \propto \chi^2(2s-1), \tag{A8}$$

where $s$ is the Hilbert space dimension

The left-hand side of Eq. (A8), which describes the level of state vector information fluctuations, is a $\chi^2$ distribution with $2s-1$ degrees of freedom.

The validity of the analytical expression (A8) is justified by the results of numerical modeling and observed data. Similarly to Eq. (A4), let us introduce the transformation of a complex state vector to a real vector of double length:

$$c=\begin{pmatrix} c_1 \\ \vdots \\ c_s \end{pmatrix} \rightarrow \xi=\begin{pmatrix} c_1^{(1)} \\ \vdots \\ c_s^{(1)} \\ c_1^{(2)} \\ \vdots \\ c_s^{(2)} \end{pmatrix}. \tag{A9}$$

It can be shown that the information carried by a state vector is equal to the doubled total number of observations in all processes:

$$\langle \xi|H|\xi\rangle = 2n, \tag{A10}$$

where $n=\Sigma_\nu k_\nu$.

Then, the $\chi^2$ criterion can be expressed in a form invariant to the state vector scale (let us recall that we consider a non-normalized state vector):

$$\frac{\langle \delta\xi|H|\delta\xi\rangle}{\langle \xi|H|\xi\rangle} \propto \frac{\chi^2(2s-1)}{4n}. \tag{A11}$$

Relation (A11) describes the distribution of relative information fluctuations. It shows that the relative information uncertainty of a quantum state decreases with the number of observations as $1/n$.

The mean value of relative information fluctuations is

$$\overline{\frac{\langle \delta\xi|H|\delta\xi\rangle}{\langle \xi|H|\xi\rangle}} = \frac{2s-1}{4n}. \tag{A12}$$

The information fidelity may be introduced as a measure of correspondence between the theoretical state vector and its estimate:

$$F_H = 1 - \frac{\langle \delta\xi|H|\delta\xi\rangle}{\langle \xi|H|\xi\rangle}. \tag{A13}$$

Correspondingly, the value $1-F_H$ is the information loss.

The convenience of $F_H$ relies on its simpler statistical properties compared to the conventional fidelity $F$. For a system where statistical fluctuations dominate, fidelity is a random value, based on the $\chi^2$ distribution:

$$F_H = 1 - \frac{\chi^2(2s-1)}{4n}, \tag{A14}$$

where $\chi^2(2s-1)$ is a random value of $\chi^2$ type with $2s-1$ degrees of freedom.

Information fidelity asymptotically tends to unity when the sample size is growing up. Complementary to statistical fluctuations noise leads to a decrease in the informational fidelity level compared to the theoretical level (A14).


[1] H. Bechmann-Pasquinucci and W. Tittel, Phys. Rev. A **61**, 062308 (2000).
[2] H. Bechmann-Pasquinucci and A. Peres, Phys. Rev. Lett. **85**, 3313 (2000).
[3] N. J. Cerf, M. Bourennane, A. Karlsson, and N. Gisin, Phys. Rev. Lett. **88**, 127902 (2002).
[4] C. Brukner, M. Zukowski, and A. Zeilinger, Phys. Rev. Lett. **89**, 197901 (2002).
[5] A. V. Burlakov and D. N. Klyshko, JETP Lett. **69**, 839 (1999).
[6] A. V. Burlakov and M. V. Chekhova, JETP Lett. **75**, 432 (2002).
[7] R. T. Thew, A. Acin, H. Zbinden, and N. Gisin, e-print quant-ph/0307122.
[8] A. Mair, A. Vaziri, G. Weihs, and A. Zeilinger, Nature (London) **412**, 313 (2001); A. Vaziri, G. Weihs, and A. Zeilinger, Phys. Rev. Lett. **89**, 240401 (2002).
[9] G. Molina-Terriza, J. P. Torres, and L. Torner, Opt. Commun. **228**, 155 (2003).
[10] N. K. Langford *et al.*, Phys. Rev. Lett. **93**, 053601 (2004).
[11] J. C. Howell, A. Lamas-Linares, and D. Bouwmeester, Phys. Rev. Lett. **88**, 030401 (2002).
[12] A. V. Burlakov, M. V. Chekhova, D. N. Klyshko, O. A. Karabutova, and S. P. Kulik, Phys. Rev. A **60**, R4209 (1999).
[13] Yu. I. Bogdanov, M. V. Chekhova, G. A. Maslennikov, S. P. Kulik, M. K. Tey, and C. H. Oh, e-print quant-ph/0405169.
[14] A. V. Burlakov, M. V. Chekhova, L. A. Krivitsky, S. P. Kulik, and G. A. Maslennikov, Opt. Spectrosc. **94**, 684 (2003).
[15] Yu. I. Bogdanov, L. A. Krivitsky, and S. P. Kulik, JETP Lett. **78**, 352 (2003).
[16] L. A. Krivitsky, S. P. Kulik, A. N. Penin, and M. V. Chekhova, JETP **97**, 846 (2003).
[17] Yu. I. Bogdanov, Opt. Spectrosc. **96**, 668 (2004); e-print quant-ph/0303014.
[18] A. G. White, D. F. V. James, P. H. Eberhard, and P. G. Kwiat, Phys. Rev. Lett. **83**, 3103 (1999).
[19] D. F. V. James, P. G. Kwiat, W. J. Munro, and A. G. White, Phys. Rev. A **64**, 052312 (2001).
[20] R. T. Thew, K. Nemoto, A. G. White, and W. J. Munro, Phys. Rev. A **66**, 012303 (2002).
[21] J. B. Altepeter, D. Branning, E. Jeffrey, T. C. Wei, P. G. Kwiat, R. T. Thew, J. L. O'Brien, M. A. Nielsen, and A. G. White, Phys. Rev. Lett. **90**, 193601 (2003).
[22] D. N. Klyshko, *Photons and Nonlinear Optics* (Gordon and Breach, New York, 1988).
[23] A. V. Belinsky and D. N. Klyshko, Laser Phys. **4**, 663 (1994).
[24] Arvind, K. S. Mallesh, and N. Mukunda, J. Phys. A **30**, 2417 (1997).
[25] D. N. Klyshko, JETP **84**, 1065 (1997).

[26] G. M. D'Ariano, M. G. Paris, and M. F. Sacchi, Adv. Imaging Electron Phys. **128**, 205 (2003).
[27] K. Vogel and H. Risken, Phys. Rev. A **40**, 2847 (1989).
[28] T. Opatrny, D.-G. Welsch, and W. Vogel, e-print quant-ph/9703026.
[29] Z. Hradil, Phys. Rev. A **55**, R1561 (1997).
[30] K. Banaszek, Phys. Rev. A **57**, 5013 (1998).
[31] K. Banaszek, G. M. D'Ariano, M. G. A. Paris, and M. F. Sacchi, Phys. Rev. A **61**, 010304 (2000).
[32] G. M. D'Ariano, M. G. A. Paris, and M. F. Sacchi, Phys. Rev. A **62**, 023815 (2000).
[33] D. T. Smithey, M. Beck, and M. G. Raymer, Phys. Rev. Lett. **70**, 1244 (1993).
[34] G. M. D'Ariano and M. G. A. Paris, J. Opt. B: Quantum Semiclassical Opt. **2**, 113 (2000).
[35] P. Bushev, V. Karassev, A. Masalov, and A. Putilin, Opt. Spectrosc. **91**, 558 (2001).
[36] D. F. V. James, P. G. Kwiat, W. J. Munro, and A. G. White, Phys. Rev. A **64**, 052312 (2001).
[37] F. De Martini, G. M. D'Ariano, A. Mazzei, and M. Ricci, e-print quant-ph/0207143.
[38] H. Cramer, *Mathematical Methods of Statistics* (Princeton University Press, Princeton, 1946).
[39] M. G. Kendall and A. Stuart, *The Advanced Theory of Statistics*, 4th ed. (Griffin, London, 1977).
[40] Yu. I. Bogdanov, G. A. Maslennikov, S. P. Kulik, L. C. Kwek, M. K. Tey, and C. H. Oh (unpublished).
[41] Y. H. Shih and A. V. Sergienko, Phys. Lett. A **191**, 201 (1994); **186**, 29 (1994); M. H. Rubin, D. N. Klyshko, Y. H. Shih, and A. V. Sergienko, Phys. Rev. A **50**, 5122 (1994).